

# Can We Identify Unknown Audio Recording Environments in Forensic Scenarios?

Denise Moussa\*, Germans Hirsch\*, Christian Riess, *Senior Member, IEEE*,

**Abstract**—Audio recordings may provide important evidence in criminal investigations. One such case is the forensic association of the recorded audio to the recording location. For example, a voice message may be the only investigative cue to narrow down the candidate sites for a crime.

Up to now, several works provide tools for closed-set recording environment classification under relatively clean recording conditions. However, in forensic investigations, the candidate locations are case-specific. Thus, closed-set tools are not applicable without retraining on a sufficient amount of training samples for each case and respective candidate set. In addition, a forensic tool has to deal with audio material from uncontrolled sources with variable properties and quality.

In this work, we therefore attempt a major step towards practical forensic application scenarios. We propose a representation learning framework called EnvId, short for environment identification. EnvId avoids case-specific retraining. Instead, it is the first tool for robust few-shot classification of unseen environment locations. We demonstrate that EnvId can handle forensically challenging material. It provides good quality predictions even under unseen signal degradations, environment characteristics or recording position mismatches.

Our code and datasets will be made publicly available upon acceptance.

**Index Terms**—audio forensics, representation learning, environment identification.

## I. INTRODUCTION

Audio forensics plays an important part in criminal investigations. Audio recordings can be evidence themselves, or an analysis of their signal characteristics can contribute to evidence or provide investigative cues [47].

One such characteristic is the reverberation in an audio recording. Reverberation, most generally described, results from reflections of sound waves at the recording location. For example, when a recording is made of a sound that originates next to a wall (consider, e.g., the breaking of a glass), then the microphone records the primary sound that travels directly from the origin to the microphone, and a reflection of that sound from the wall. A simple computational model for reverberation is the convolution of a clean signal with an acoustic impulse response (AIR).

In principle, any enclosed environment or any obstacle contributes to a reverberation signature. One can invert this consideration to obtain a forensic cue: the reverberation in an audio recording characterizes the recording location. The inverse mapping of reverberation to environment geometry and composition is not unique, but from a practical point of view it is oftentimes sufficiently distinctive to support or reject hypotheses that a recording has been made in one out of a set

of specific environments. Such a question is of high practical relevance for the reconstruction of crime scenes and the course of events in a crime [47].

Two additional challenges increase the difficulty of forensic investigations. First, it is impractical to collect extensive training data on a case-by-case basis. If example data is available for a set of case-related environments, then it can for practical reasons only stem from a limited acquisition. Second, forensic investigations oftentimes have to work with audio samples from uncontrolled sources, i.e., the data can be in almost any encoding or quality. This imposes high requirements on the robustness of the analysis tools.

There exist works that aim to perform environment identification with analytic tools [3], [26], [33]. However, it is generally difficult to appropriately model the complexity of real-world audio conditions in an analytic model. As a consequence, deep learning (DL) tools have been increasingly explored to learn signal characteristics from example data for this and other forensic tasks [1], [2], [4], [27], [31], [44]. Nevertheless, existing methods for environment identification still impose relatively strict constraints. For example, many works perform environment identification in a closed-set scenario, i.e., the network must be specifically trained for relevant target environments [1], [3], [25], [26], [30], [31], [33]. While this is feasible, e.g., for smart home assistants, it does not meet the requirements for forensic applications. Oftentimes the analysis is performed only on relatively clean recordings [3], [23], [25], [30], [31], [33] or on noisy environment where the noise distribution is already known at training time [1], [26].

In this work, we aim to make a substantial step forward towards forensic environment identification under practical constraints. We propose a representation learning framework that performs environment classification, where the embedding space also allows the regression of environment parameters. Environment classification is realized as few-shot learning, i.e., it is not necessary to retrain the representation for a new case, but instead only a few sample audio recordings are required from the candidate environments. Additionally, the proposed method is extensively trained on mixed-quality data, and as a consequence very relaxed in its assumptions on the quality of the input data. We extensively evaluate the proposed approach in difficult scenarios, include training-test mismatches, unseen noise and lossy compression. This work also evaluates the impact of specific microphone positions on few-shot inference. The influence of the microphone position is oftentimes overlooked in academic research, but it can be a relevant source of error in practice.

We denote the proposed framework as “EnvId”, as an abbreviation for “environment identification”. We hope that

\* Authors contributed equally to this work.

EnvId will set a new standard for environment identification from data in the wild, and set a baseline for further research in this direction<sup>1</sup>.

The paper is organized as follows. Section II reviews related work on environment identification. In Sec. III we present the proposed EnvId framework, and the data generation pipeline for simulating challenging forensic scenarios. Extensive experiments are performed in Sec. IV, and Sec. V concludes the work.

## II. RELATED WORK

Various methods have been proposed that either perform environment identification in constrained closed-set scenarios or that estimate environmental properties from audio signals. These methods are mostly evaluated on good quality data without a significant mismatch in the training and test distribution.

Many works address the classification of recording environments of single channel audio samples from a known (closed) set of classes [1], [3], [24]–[26], [30], [31], [33].

Some methods train traditional classifiers like Gaussian Mixture Models (GMMs) or Support Vector Machines (SVMs) on hand-crafted features that serve as acoustic fingerprints for the respective environments [3], [24]–[26], [30], [33]. More recent methods oftentimes use DL for the closed-set classification. Papayiannis *et al.* [31] show the superiority of deep features of a convolutional recurrent neural network (CRNN) as opposed to custom, analytic features, while Azimi *et al.* [1] use the deep features of pre-trained neural networks (NNs) for speaker identification as input to an SVM. The closed-set scenario is a useful assumption in smart home environments, where it is possible to train on the same recording environments that are queried at test time [1], [31]. However, the forensic task of environment identification is by design a problem that has to operate with unknown recording locations at test time. Hence, existing closed-set methods are not applicable. For this reason, we instead approach the problem as a few-shot classification task. Few-shot learning has already been successfully explored for audio classification to distinguish between signals of different content like, *e.g.*, background music, bird voices or human speech [15], [42], [43], [46], but not for the identification of audio recording environments.

Other works focus on the estimation of specific environment parameters from single channel audio samples [6], [9]–[13], [16], [23]. Moore *et al.* [23] use analytical models to estimate the geometry of 2-D rectangular rooms while more recent approaches employ deep features and directly regress characteristic environment parameters with NNs. For example, many works target the estimation of  $RT_{60}$ , *i.e.* the time until the AIR energy decays by 60 db, or the volume of some space [6], [10]–[13], [16]. However, also other parameters were investigated, like  $C_{50}$ , *i.e.* the ratio between the first 50 ms of a signal and its remaining late energy [9], [13]. From a forensic point of view, the estimation of specific environment characteristics might unveil important cues. However, environment identification

from estimated environment parameters is by design a two-stage process, and as such relatively prone to errors: the parameters themselves are only estimates and subject to possible confusions, overlap, or just estimation errors, and a subsequent environment identification may add further estimation errors. Still, the task may become relevant if the police does not have a hypothesis about candidate locations, but aims to characterize the recording location for further investigations, such as a coarse estimate of the volume of a room. Thus, we demonstrate that our framework is capable of environment parameter estimation, but put our primary focus on few-shot learning to directly identify recording locations.

The robustness to signal degradations is an underexplored topic in research on room identification. Several works experiment on quasi clean audio signals [3], [23], [25], [30], [31], [33], others simulate noise degradations, but use identical distributions in both the training and the test sets [1], [6], [9]–[11], [16], [26]. In contrast to previous research, we set the focus on audio material in forensic investigations which is usually ‘in-the-wild’ data of uncontrolled characteristics. We thus evaluate under significant training and test set mismatches, as in practice, the audio signal might be heavily impacted by unknown degradation factors. We include varying noise distortions which can be expected from arbitrarily noisy environments or distortions introduced by low-cost acquisition devices. We also evaluate the practically important case of lossy audio compression and also re-compression, which both have not been addressed in previous works to our knowledge.

Additionally, we analyze the impact of recording position mismatches for few-shot classification. Some works on closed-set environment classification evaluate training/test mismatches of microphone positions, where the actual positions are not further documented [3], [26]. Here, we take a further step forward and give first insights into the influence of specific microphone positions on few-shot inference.

## III. METHODS

The proposed framework for few-shot environment identification and parameter estimation is presented in Sec. III-A. The associated data generation pipeline is presented in Sec. III-B.

### A. The EnvId Framework

EnvId is designed as an end-to-end trainable framework that handles joint few-shot environment identification and environmental parameter regression. At its core, EnvId aims to learn a representation (or embedding) in which distances enable a distinction of recording locations: distances between vectors from the same recording location are smaller than distances between vectors from any other recording location. The trained embedding can then be used to query the affinity of an *unseen* sample to *unseen* reference recording environments. Either the closest matching environment is returned, or the input is rejected if the distance to all candidates is too large.

Technically, the representation learning is achieved with Prototypical Networks [37], a representation learning approach that enables few-shot classification. Prototypical Networks have primarily been used for computer vision tasks, but

<sup>1</sup>Code and data will be made publicly available upon acceptance of the paper.

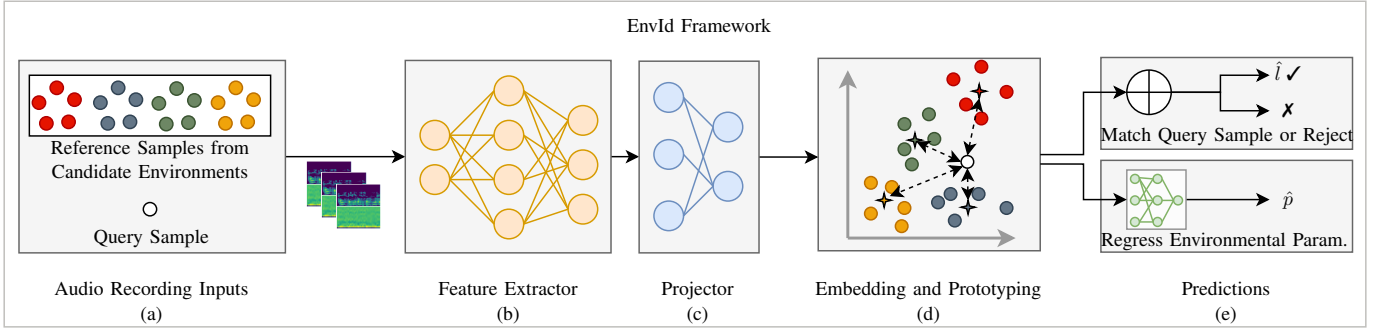


Fig. 1: Our end-to-end trainable EnvId framework for joint few-shot environment identification and blind parameter regression from ‘in-the-wild’ recording samples. The framework consists of a neural feature extractor (b) and projector (c) to process and map the input samples (a) to the learnable, metric embedding space (d). The audio representations in the metric space can both be used for the identification of environments, and the regression of environment parameters (e).

some studies on audio classification also demonstrate their effectiveness on audio signals [15], [42], [43], [46].

The main task for the framework is environment identification. Here, the task is to assign an audio recording to a specific recording location from a set of reference candidates  $\mathcal{R}_l = \{l_1, l_2, \dots, l_M\}$  never seen in training, or to reject the assignment if the recording is from a different location. In a given forensic case, it may happen that a candidate set  $\mathcal{R}_l$  is not available, i.e., that an analyst has no specific hypothesis about the recording location. In this case, the framework also enables a secondary task, namely the blind regression of scalar environmental parameters from input samples. Such an estimate can provide important hints about the nature of the unknown recording location.

A high-level overview of the EnvId framework is shown in Fig. 1. The framework learns the representation by training on reference recordings from candidate locations (Fig. 1(a)), from which features are extracted (Fig. 1(b)) and projected into the representation space (Fig. 1(c)), where prototypes represent the locations (Fig. 1(d)). This representation provides a suitable metric space to match a new (unseen) query sample to (unseen) candidate locations  $\mathcal{R}_l$  (Fig. 1(e) top). This matching constitutes the few-shot identification of the recording environment. If no candidate locations  $\mathcal{R}_l$  are available, then specific environmental parameters can be blindly regressed with an additional fully-connected network. (Fig. 1(e) bottom). These steps are presented in greater detail in the following paragraphs.

1) *Audio Recording Inputs (Fig. 1(a))*: The input is transformed to dense frequency representations, as it is commonly done in audio processing [2], [27], [31], [35]. In detail, we compute the Mel spectrogram [22] and the Mel frequency cepstral coefficients (MFCCs) [22] and concatenate the coefficients of both representations into one feature vector. The Mel spectrograms are computed with torchaudio [39] with a window size and FFT size of 1024 bins, a stride of 512, and 256 Mel filter banks. The MFCCs uses 20 coefficients and is computed from the spectrogram.

2) *Feature Extraction (Fig. 1(b))*: A deep feature vector of  $D$  dimensions is extracted from an input audio recording.

We recommend here a slim convolutional neural network

(CNN) backbone that we refer to as Gamper\*. It is a variation of the CNN feature extractor by Gamper *et al.* [10]. Different than the original work, we recommend to use uniform  $3 \times 3$  filter kernels in all layers instead of large kernel dimensions in the time domain, since this degraded results in early experiments.

However, also any other custom end-to-end trainable feature extractor can be used for this stage, and we demonstrate the performances of various other networks in the associated evaluation in Sec. IV-B.

3) *Feature Projection (Fig. 1(c)-(d))*: The extracted features are projected to the metric embedding space of fixed size. For our studies, we use a simple fully connected layer for the mapping  $\mathbb{R}^D \mapsto \mathbb{R}^E$  of the deep features’ dimension  $D$  to the embedding dimension  $E$ . While the embedding dimension can be varied, we use  $E = 256$  throughout all experiments, as we observed in early studies with  $2^6 \leq E \leq 2^9$  that smaller  $E$  led to worse embedding space results while larger  $E$  did not show any advantage.

4) *Embedding Space Optimization (Fig. 1(e))*: The representation in the embedding space can either be used for environment identification (Fig. 1(e) top) or for parameter regression (Fig. 1(e) bottom). The regression requires an additional output layer, and both tasks are trained with different losses, which is described in greater detail below.

The idea of a Prototypical Network [37] is to assign a query sample to a so-called prototype of some class. Thus, in our case, a prototype represents a specific recording location. Prototypical Networks can match inputs to prototypes of classes during testing that are entirely *unseen*, i.e., neither samples from the same class as the query sample nor samples from the same class as the reference samples forming the prototype were part of the training set. This is a big advantage over standard closed-set classifiers. It enables law enforcement to deploy a trained network, and to operate it on actual case work with case-specific queries and case-specific candidate locations without retraining.

More in detail, Prototypical Networks provide an  $E$ -dimensional representation space that enables few-shot learning. At inference time, few samples of each candidate location  $l_m$  are projected into the embedding space and averaged to

form one prototype  $\mathbf{p}_{l_m}$  per location. Then, the Euclidean distance between a query sample  $\mathbf{q}$  and each prototype is evaluated,

$$d(\mathbf{p}_{l_m}, \mathbf{q}) = \|\mathbf{p}_{l_m} - \mathbf{q}\| . \quad (1)$$

A query can be rejected if there is no prototype within a reasonably short Euclidean distance (*cf.* Sec. IV-B4). Otherwise, the likelihood that a query sample belongs to a prototype is given by the softmax function over the distances of all classes

$$p(\mathbf{q} = l_m | \mathbf{X}) = \frac{\exp(d(\mathbf{p}_{l_m}, \mathbf{q}))}{\sum_N \exp(d(\mathbf{p}_{l_m}, \mathbf{q}))} . \quad (2)$$

The learning task is to find an embedding space representation where the Euclidean distance between an unseen sample and unseen reference recordings is actually meaningful. To this end, the training is split in episodes. In each episode,  $M$  different recording locations  $l_m$  are randomly drawn from the training set, and  $K$  reference samples are randomly drawn from each of these locations. For each class, a prototype is computed as the average vector

$$\mathbf{p}_{l_m} = \frac{1}{|K|} \sum_{\mathbf{x}_k \in \mathcal{S}_{l_m}} \mathbf{x}_k , \quad (3)$$

where  $\mathcal{S}_{l_m}$  denotes the set of  $K$  samples from location  $l_m$  in the  $E$ -dimensional embedding space. The training loss is the negative log-likelihood

$$\mathcal{L}_{\text{class}} = -\log p(\mathbf{q} = l_m | \mathbf{X}) , \quad (4)$$

which is minimized for the correct location  $l_m$ .

If no reference environments are available, EnvId can also regress scalar environmental parameters from a query's embedding  $\mathbf{q} \in \mathbb{R}^E$  (Fig. 1 (e) bottom). To this end, we propose to append two linear layers with dimension  $E = 256$  and a scalar output for the estimated parameter.

The training requires samples with known environmental parameters. The loss for including the regression task for training is

$$\mathcal{L}_{\text{total}} = \mathcal{L}_{\text{class}} + \mathcal{L}_{\text{reg}} = -\log p(\mathbf{q} = l_m | \mathbf{X}) + |p_e - \hat{p}_e| , \quad (5)$$

which uses the room identification loss as in Eq. 4, and additionally the absolute deviation of the environmental parameter label  $p_e$  from its regressed prediction  $\hat{p}_e$ . Our experiments in Sec. IV-E set  $p_e$  to volume and  $\text{RT}_{60}$ , i.e. the time in which the signal energy decays by 60db.

Technically, the framework is implemented in PyTorch [32] v.1.10.2. Training is conducted on one consumer GPU, at most a RTX3090, with the Adam [19] optimizer and learning rate  $1e^{-4}$  for at maximum 300 epochs. Early stopping is applied when the validation accuracy for assigning audio samples to recording locations does not increase for 30 epochs.

### B. Generation of Almost-In-the-Wild Audio Samples

The quite unconstrained nature of in-the-wild data must be met with extensive training with diverse datasets and various training data augmentations. The specific training samples are hence created with a flexible data generation pipeline that aims to mimic in-the-wild data. We first review the theoretical model for the simulation of reverberant environments in

Sec. III-B1, and then present the proposed data generation pipeline in Sec. III-B2.

1) *Background on Reverberant Environments:* Consider an audio signal  $a(t)$  that propagates from a source into space. During propagation,  $a(t)$  may be partially reflected from objects. Such reflections cause the signal to arrive at slightly different times at a recording microphone, commonly referred to as reverberation. Reverberation can be measured an acoustic impulse response (AIR) signal  $r(t)$ . A reverberated audio signal  $s(t)$  is hence commonly modeled as a convolution

$$s(t) = r(t) * a(t) . \quad (6)$$

of  $a(t)$  with the AIR  $r(t)$ , which is the de-facto standard model for reverberation [1], [3], [25], [26], [30], [31], [33]. Hence, one can separately record reverberation-free audio signals  $a(t)$  and AIRs  $r(t)$ , and freely combine both signals into a reverberated audio signal.

2) *Data Generation Pipeline:* In the first step, shown in Fig. 2 (a), reverberant environments are simulated from anechoic speech samples and AIRs using Eq. 6.

In the second step, shown in Fig. 2 (b), noise degradation is optionally added. We follow related work that models noise as an additive signal  $n(t)$  scaled by scalar noise impact  $\alpha$  [1], [6], [9]–[11], [16], [26]. Hence, the signal becomes

$$\hat{s}(t) = r(t) * a(t) + \alpha \cdot n(t) . \quad (7)$$

Customized test scenarios are created by feeding the generator with a set of noise signals  $n(t)$  and an interval of signal-to-noise ratios (SNRs) that controls the noise strength. The generator randomly samples the noise configuration for each incoming sample.

In the third step, shown in Fig. 2 (c), lossy compression is optionally introduced as it might occur upon social media sharing, editing/re-saving or other types of data processing. This further extends the signal formation to

$$\tilde{s}(t) = f_1^C(\dots f_N^C(r(t) * a(t) + \alpha \cdot n(t))) , \quad (8)$$

where  $f_n^C(\cdot)$  with  $n \in [1, N]$  describes one out of  $N$  lossy compression operations. The framework natively supports the popular formats MP3, AMR-NB, GSM and Vorbis, and also the neural EnCodec [5] format. If compression is applied, the specific compression algorithm and strength is randomly sampled from a customisable set for each incoming sample. Re-compression is simulated by repeating this random compression process.

## IV. EXPERIMENTS

The evaluation is organized in five parts. First, Sec. IV-A lists the data sources for the experiments. Section IV-B reports EnvId's performance for different feature extractors and compares it to related work. This benchmark also justifies our proposed backbone for the remaining sections. Section IV-C explores EnvId's robustness towards unseen signal degradations, which is highly relevant for practical forensic cases. Section IV-D investigates the performance when the microphone positions differ for the reference and query samples. Section IV-E explores blind environmental parameter regression from degraded signals for volume and  $\text{RT}_{60}$ .

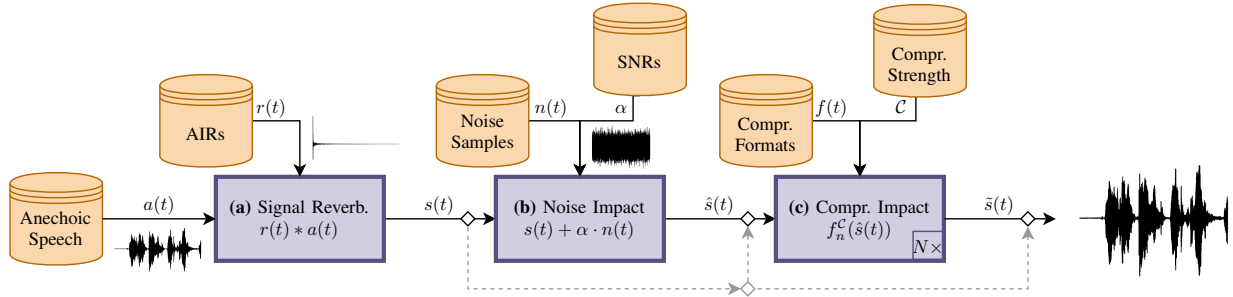


Fig. 2: Proposed pipeline for controlled simulation of real world audio recording and post-processing scenarios. Configurable sets of input signals, environments and degradations (orange) enable the creation of custom test cases. In 3 steps (purple), anechoic audio signals  $a(t)$  pass various transformations and are output in frequency representation. Dashed arrows indicate skip connections to (randomly) enable and disable degradation transformations per sample.

Data Pool	Speech $a(t)$	AIR $r(t)$
	Source: # Samples	Source: # Samples
Train	ACE [8] : 239	MIT [40] : 200
Valid.	ACE [8] : 64	MIT [40] : 20
Test	TSP [18] : 67	ACE [8] : 7
		AAIR+REV [17], [20] : 13
		MIT [40] : 20 OPENAIR [28] : 20

TABLE I: Composition of the source data pools of anechoic speech samples and AIRs for dataset generation.

#### A. Data Sources and Evaluation Dataset Composition

The single channel audio signals and AIRs in this work are collected from a total of seven freely available speech databases. The source data pools are summarized in Tab. I and further described below.

1) *Anechoic Speech Pools.*: The basis of our data are speech samples from anechoic datasets.

From the ACE corpus [8], we use 33 speech samples from 4 female speakers and from 7 male speakers with a duration between 3 s and 97 s.

From TSP, we use 87 utterances from 2 female speakers and from 2 male speakers with a duration between 1.70 s and 3.25 s. This dataset is used for testing.

All experiments operate on audio snippets of 3 s, and longer samples are split into 3 s segments. TSP has also shorter samples, which are enlarged by concatenating speech from the same speaker at silent positions. Hence, we have a total of 239/64 speech samples from the ACE [8] corpus for training and validation, and 67 clean voice snippets from TSP for testing as shown in the left column of Tab. I.

2) *AIR Pools.*: The training/validation AIR pool consists of real 200/20 AIRs from the MIT Acoustical Reverberation Scene Statistics Survey [40] (MIT) dataset. The MIT set provides diverse space categories. Small categories are, e.g., *cars* and *bathroom*, mid-size categories are, e.g., *bar*, *train*, and *hallway*, and large categories are, e.g., *theatre*, *atrium*, or *open air*.

For testing we use four separate AIR pools from the remaining MIT AIRs and from smaller databases that are described below.

The *ACE test pool* consists of the ACE AIR set of 7 rooms that is oftentimes used in related work [1], [3], [6], [9]–[12], [16], [26], [31]. The rooms are enclosed mid-size spaces of the category *lecture room*, *meeting room*, *office room* and *lobby*, with volumes between 47.3 m<sup>3</sup> and 370 m<sup>3</sup>.

The *AAIR+REV test pool* is created by combining the 7 real AIR measurements from the Aachen Impulse Response Database (AAIR) [17] with 6 high-quality simulations from the 2014 REVERB challenge (REV) [20]. AAIR provides measurements from a low-reverberant studio booth, a stairway, an office, a meeting room, two lecture rooms, and a church. It features diverse surface materials and furniture. The room volumes range between 11.9 m<sup>3</sup> and 370.8 m<sup>3</sup>, except for the church where only the floor area is reported with 570 m<sup>2</sup>. To enlarge the dataset, we sample 6 high-quality simulations from the REV set following Kinoshita *et al.* [20], where 2 rooms are from each category *small*, *medium* and *large*.

The *MIT* and *OPENAIR test pools* contain 20 AIR measurements each. The MIT [40] database provides AIRs from variable space categories while the OPENAIR [28] data mainly covers large spaces like churches, halls, auditoriums and open spaces, where the volumes (excluding open air) range between 35.2 m<sup>3</sup> and 140000 m<sup>3</sup>.

These real AIR measurements and high-quality AIR simulations represent a wide range of recording environments. The specific selected environments are listed in Tab. III and Tab. A.1, A.2, A.3 of the supplemental material.

The data generation pipeline from Sec. III-B is used to generate a training/validation set of about 48k/1.3k samples from the data pools. Hereby, each speech sample is paired with each AIR, which leads to a uniform distribution of recording examples for each available environment (Fig. 2(a)). This experiment features common quality impacts for real world scenarios. General background noise on the training set is simulated with additive white noise of a broad SNR range of  $\alpha \in [-10, 50]$  db (Fig. 2(b)). For additional compression (Fig. 2(c)), we use MP3, AMR-NB and GSM as popular formats with all available bitrate settings that control the compression strength. Thus, the input configurations to the pipeline are  $\mathcal{C}_{MP3} = \{8, 16, 24, 32, 40, 48, 56, 64, 80, 96, 112, 128\}$ ,  $\mathcal{C}_{AMR-NB} = \{4.75, 5.15, 5.9, 6.7, 7.4, 7.95, 10.2, 12.2\}$  and  $\mathcal{C}_{GSM} = \{13\}$ , since GSM only operates with constant bitrate.

Feature Extractor	Params	ACE [8]		AAIR+REV [17], [20]		MIT [40]		OPENAIR [28]		
		$\mu \pm \sigma$	max	$\mu \pm \sigma$	max	$\mu \pm \sigma$	max	$\mu \pm \sigma$	max	
Guessing chance		0.1430		0.0769		0.0500		0.0500		
<b>Related Work — CRNNs:</b>										
Papayiannis [31]	2.66 M	0.6768 $\pm$ 0.0314	0.7122	0.6866 $\pm$ 0.0166	0.7072	0.7134 $\pm$ 0.0068	0.7239	0.5652 $\pm$ 0.0274	0.5985	
GamperCRNN [9]	1.25 M	0.7062 $\pm$ 0.0336	0.7676	0.7362 $\pm$ 0.0308	0.7738	0.7439 $\pm$ 0.0181	0.7761	0.5551 $\pm$ 0.0321	0.6157	
Deng/Götz [6], [12]	5.49 M	0.8068 $\pm$ 0.0271	0.8401	0.7614 $\pm$ 0.0564	0.8427	0.6755 $\pm$ 0.0647	0.7463	0.6204 $\pm$ 0.0795	0.7373	
<b>Related Work — CNNs:</b>										
VGGVox [1], [29]	11.65 M	0.4827 $\pm$ 0.0079	0.4947	0.5362 $\pm$ 0.0184	0.5637	0.5497 $\pm$ 0.0065	0.5567	0.4727 $\pm$ 0.0201	0.5037	
Genovese/Ick [11], [16]	0.19 M	0.8196 $\pm$ 0.1028	0.8721	0.7715 $\pm$ 0.0841	0.8220	0.7340 $\pm$ 0.1149	0.8022	0.6937 $\pm$ 0.1064	0.7448	
ThinResnet [1], [45]	11.72 M	0.8499 $\pm$ 0.0178	0.8806	0.8583 $\pm$ 0.0190	0.8783	0.8257 $\pm$ 0.0054	0.8328	0.6907 $\pm$ 0.0329	0.7388	
Götz [13]	3.86 M	0.9416 $\pm$ 0.0218	0.9616	0.9150 $\pm$ 0.0355	0.9518	0.8236 $\pm$ 0.0454	0.8679	0.8187 $\pm$ 0.0501	0.8754	
GamperCNN [10]	3.43 M	0.9467 $\pm$ 0.0189	0.9638	0.9254 $\pm$ 0.0291	0.9506	0.8345 $\pm$ 0.0419	0.8687	<b>0.8240</b> $\pm$ 0.0486	0.8709	
<b>Standard Vision CNNs:</b>										
RegNetY-400mf [34]	28.23 M	0.7211 $\pm$ 0.0441	0.7868	0.7724 $\pm$ 0.0307	0.8129	0.7334 $\pm$ 0.0387	0.7851	0.6163 $\pm$ 0.0400	0.6649	
EffNet-B0 [38]	12.85 M	0.7318 $\pm$ 0.0303	0.7868	0.8101 $\pm$ 0.0157	0.8301	0.7939 $\pm$ 0.0116	0.8067	0.6300 $\pm$ 0.0191	0.6642	
EffNet-B2 [38]	17.43 M	0.7548 $\pm$ 0.0199	0.7932	0.8057 $\pm$ 0.0278	0.8542	0.8078 $\pm$ 0.0121	0.8291	0.6639 $\pm$ 0.0209	0.6925	
RegNetY-800mf [34]	43.75 M	0.7646 $\pm$ 0.0187	0.7846	0.7929 $\pm$ 0.0114	0.8140	0.7640 $\pm$ 0.0213	0.7888	0.6436 $\pm$ 0.0141	0.6604	
ResNet-18 [14]	11.30 M	0.8171 $\pm$ 0.0345	0.8593	0.8200 $\pm$ 0.0276	0.8588	0.8124 $\pm$ 0.0111	0.8269	0.6778 $\pm$ 0.0348	0.7336	
ResNet-50 [14]	24.03 M	0.8175 $\pm$ 0.0113	0.8316	0.8361 $\pm$ 0.0110	0.8485	0.8045 $\pm$ 0.0106	0.8216	0.6840 $\pm$ 0.0076	0.6925	
ConvNeXt-Tiny [21]	28.01 M	0.8618 $\pm$ 0.0112	0.8806	0.7986 $\pm$ 0.0137	0.8129	0.7658 $\pm$ 0.0190	0.8000	0.7022 $\pm$ 0.0118	0.8000	
<b>Standard Transformers:</b>										
Transf. Enc. [41]	19.19 M	0.4034 $\pm$ 0.0394	0.4670	0.4693 $\pm$ 0.0388	0.5385	0.4663 $\pm$ 0.0141	0.4903	0.4227 $\pm$ 0.0227	0.4545	
ViT-Small [7]	86.08 M	0.4968 $\pm$ 0.0350	0.5437	0.5146 $\pm$ 0.0234	0.5408	0.4922 $\pm$ 0.0113	0.5045	0.4813 $\pm$ 0.0128	0.5015	
<b>Proposed Backbone:</b>										
Gamper*	3.86 M	<b>0.9557</b> $\pm$ 0.0076	0.9701	<b>0.9375</b> $\pm$ 0.0047	0.9449	<b>0.8712</b> $\pm$ 0.0164	0.8903	0.8131 $\pm$ 0.0188	0.8358	

TABLE II: Mean and maximum accuracy values of 5 training runs for all backbones and datasets under single compression and noise degradation. The best (bold), second best (underlined) and third best (italic) model results are highlighted. The parameter size includes backbone and EnvId trainable weights. We provide an own custom backbone (last row) as strong baseline for further research.

The test data pools are used to generate 4 test datasets with recording locations from different sources. Also here, each anechoic test sample is convolved with all available AIRs from the test pool. For the experiment in Sec. IV-B, noise and compression settings are identical between training and testing. The other experiments may vary the test configuration, which is described in the respective Sections below.

### B. Comparisons to Various Baselines and Backbones

The proposed framework is compared to feature extractors from related works and popular standard NN architectures. The task is few-shot forensic environment identification, and we use the training/test datasets as described in the previous Section. This experiment is split in three parts, where we first perform a broad comparison in Sec. IV-B2. Then, we use only the three best performing feature extractors and evaluate their generalization ability in Sec. IV-B3 and their open-set rejection ability in Sec. IV-B3.

1) *Evaluation Protocol:* The comparison covers 8 neural feature extractors that we implement from 11 published works. Three extractors are based on CRNNs, which we denote as Papayiannis [31], GamperCRNN [10], and Deng/Götz [6], [12]. Five extractors are based on CNNs, which we denote as VGGVox [1], [29], Genovese/Ick [11], [16], ThinResnet [1], [45], Götz [13], and GamperCNN [9]. Additionally, 7 standard CNNs from the RegNet [34], EffNet [38], ResNet [14] and ConvNext [21] families and two standard Transformer models [7], [41] are considered, because standard architectures oftentimes showed good transfer learning capabilities in var-

ious forensic and steganalytic tasks. Our proposed backbone is a variation of GamperCNN that we denote as Gamper\* (cf. Sec. III-A).

Each of the evaluated models is integrated into EnvId in two steps. The final classification/regression layers (if present) are removed, and the remaining layers (Fig. 1 (b)) are linked to EnvId’s projector layer (Fig. 1 (c)). The projector reduces the dimensionality of the model to  $E = 256$ , which proved to be sufficiently large for our purpose (cf. Sec. III-A). Missing parameter configurations in related methods are supplemented with the respective standard values from PyTorch [32].

For a representative comparison, we conduct 5 EnvId training runs with random weight initialization for each feature extractor and report the mean and best model accuracy per test set. For the computation of good-quality prototypes in the embedding space (cf. Sec. III-A), we randomly sample a subset of  $N_s = 15$  samples for  $L = 10$  recording environment classes per episode.

2) *Comparison of Feature Extractors:* Table II shows the evaluation results. The first row lists the random guessing chance per test set, the following rows list the results per feature extractor and test set grouped by the underlying technique. Several insights can be drawn from these results. Overall, the CNN feature extractors Götz and GamperCNN and the proposed Gamper\* perform best. These networks are relatively small, with less than 4 million parameters each. Nevertheless, they outperform the much more complex CRNN extractors and various standard models with a much larger number of parameters. It is particularly notable that the Transformer

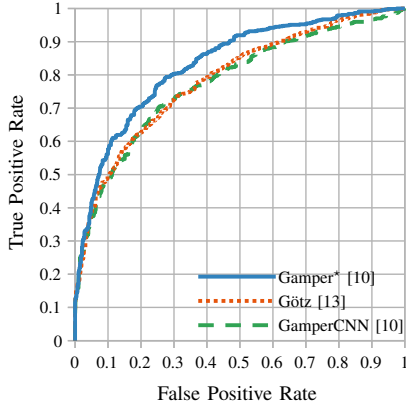


Fig. 3: ROC curve on the MIT [40] test set for rejecting samples that do not match any reference recording location.

models achieve only a quite low performance.

We hypothesize that the benefits from large vision nets and Transformers might potentially become accessible with even larger training datasets. However, due to the very promising results with efficient and slim CNNs models with short training times, we did not further investigate this direction.

For reference, the F1-Score, precision, and recall for all recording locations in all 4 test sets for Gamper\* is provided in the supplemental material.

3) *Difficult Cases in Few-Shot Generalization*: The results in Tab. II show that OPENAIR is the most difficult test set. OPENAIR consists mainly of large, strongly reverberant locations like churches, cathedrals and halls, which are only sparsely covered in the training set. In this Section, we further characterize that sparsity and the associated challenge to generalize to such queries.

One indication for the difficulty to generalize to the OPENAIR test set provides the Pearson correlation coefficient between the AIRs in the training and test sets. Here, the Pearson correlation coefficients for the ACE, AAIR+REV, and MIT test sets are 0.5555, 0.3162 and 0.5844, whereas it is only 0.2375 for the OPENAIR test set.

Also at the level of individual AIRs it is possible to observe the impact of differences in the training and test distributions. To this end, we limit the examination to the three best performing backbones GamperCNN, Götz, and Gamper\*, and examine the F1 score per space category on OPENAIR. The F1 scores of Gamper\* for all test set environments are listed in Tab. III in descending order. All three models perform worst on the same 5 church, cathedral, and hall environments (bottom part of Tab. III). For these 5 worst environments, the F1-Score is only 0.7511, 0.7083, and 0.6202 for GamperCNN, Götz, and Gamper\*. Without these 5 locations, the F1 scores for the remaining locations are much higher at 0.9098, 0.9282, and 0.8864, respectively.

The proposed Gamper\* performs slightly worse than GamperCNN and Götz on OPENAIR locations, which shows the contradicting goals of specialization and generalization. However, all results are overall quite robust, given that the tested AIRs are considerably different from the training data.

4) *Open-Set Matching: Rejection of Unknown Environments*: In several important practical use cases, it is helpful if a system can indicate that an input does not match any of the reference locations. To our knowledge, this task is not addressed in related works. EnvId’s rejection mechanism is straightforward: an input is rejected if its distance to all available prototypes exceeds a threshold. The specific choice of rejection threshold depends on practical requirements, *e.g.*, whether a higher recall or lower false positive rate is required. To show the general rejection ability, we calculate the receiver operator characteristic (ROC) for the three best performing backbones GamperCNN, Götz, and Gamper\* on the large test set of MIT AIRs. From the 20 available recording environment classes, we keep all samples as test inputs, but randomly sample only 10 locations as reference candidates.

Fig. 3 shows the results. Gamper\* performs best by some margin, but nevertheless there is room for improvement. We hence see this as a possibility for further research in the future.

### C. Robustness to Number of Prototypes and Unseen Signal Degradations

This Section provides further experiments to characterize EnvId’s robustness. All experiments use the best performing backbone Gamper\*. We first evaluate the robustness with respect to the number of few-shot prototypes for inference, and then evaluate the robustness with respect to unseen multiple compressions, unseen compression codecs, and unseen background noise.

1) *Required Number of Prototypes*: EnvId requires a few reference samples for identifying a recording environment. There are no strict constraints on the number of reference samples. From a theoretical perspective it is reasonable to claim that “more data is better”. However, in practice, the question of a lower limit on the number of required samples is relevant as data collection can be tedious. Figure 4 portrays the accuracy of EnvId with the best performing feature extractor Gamper\* on the 4 test sets w.r.t.  $K \in [1, 15]$ . For ACE and AIR+REV based sets, already  $K = 1$  reference sample provides a good prototype and locations of MIT can be stably identified with  $K = 2$  reference samples. OPENAIR, where the recording location characteristics deviate the most from our training data, requires  $K = 10$  to yield stable prototypes. This shows that the number of reference samples that need to be collected in practice depends on the embedding space quality for the respective environmental characteristics. Analogous to Sec IV-B3, these findings emphasize the importance of analyzing training data for weakly covered environmental characteristics.

2) *Multiple Compression Runs*: When audio messages are shared over the internet, the signal might be recompressed multiple times. To analyze such situations, the data pipeline is configured to perform several compressions per test sample.

The experiments are performed with Gamper\* trained on synthetic white noise and only single compression as described in Sec. IV-B1. The evaluation is performed on the MIT-based test set from Tab. II, since it is one of our larger sets and contains a diverse distribution of recording locations from

OPENAIR Class Label [28]	Volume [28]	Space Category [28]	F1-Score	Precision	Recall
Live Room	35.2 m <sup>3</sup>	Recording Studio	0.9771	1.0000	0.9552
Falkland Palace Bottle Dungeon	-	Chamber	0.9692	1.0000	0.9403
Innocent Railway Tunnel Entrance	13000 m <sup>3</sup>	-	0.9545	0.9692	0.9403
Koli National Park Summer	-	Open Air	0.9466	0.9688	0.9254
Stairwell	-	Hall	0.9343	0.9143	0.9552
Arthur Sykes Rymer Audit. Univ. York	1560 m <sup>3</sup>	Auditorium	0.9118	0.8986	0.9254
Spokane Woman’s Club	1600 m <sup>3</sup>	Auditorium, Ballroom, Hall	0.9078	0.8649	0.9552
Dixon Studio Theatre Univ. York	908.23 m <sup>3</sup>	Theater	0.9065	0.8750	0.9403
Council Chamber	1140 m <sup>3</sup>	Chamber	0.8690	0.8077	0.9403
Alcuin College Univ. York	21000 m <sup>3</sup>	Open Air	0.8514	0.7778	0.9403
Falkland Tennis Court	2300 m <sup>3</sup>	Open Air, (Sports) Hall	0.8406	0.8169	0.8657
Central Hall Univ. York	8000 m <sup>3</sup>	Auditorium, Hall	0.8366	0.7442	0.9552
Lady Chapel St Alban’s Cathedral	-	Cathedral	0.8227	0.7838	0.8657
Jack Lyons Concert Hall Univ. York	-	Concert Hall	0.8000	0.7436	0.8657
Heslington Church	2000 m <sup>3</sup>	Church	0.7680	0.8276	0.7164
Baptist Nashville Balcony	-	Church	0.7445	0.7286	0.7612
Nuclear Reactor Hall	3500 m <sup>3</sup>	Hall	0.7111	0.7059	0.7164
York Minster	140000 m <sup>3</sup>	Cathedral	0.5872	0.7619	0.4776
Terry’s Warehouse	4500 m <sup>3</sup>	Hall	0.5455	0.6977	0.4478
Sportscentre	9000 m <sup>3</sup>	(Sports) Hall	0.5128	0.6000	0.4478

TABLE III: F1-Score, precision and recall results per environment of our EnvId framework with Gamper\* backbone on the OPENAIR [28] test set under single compression and noise degradation.

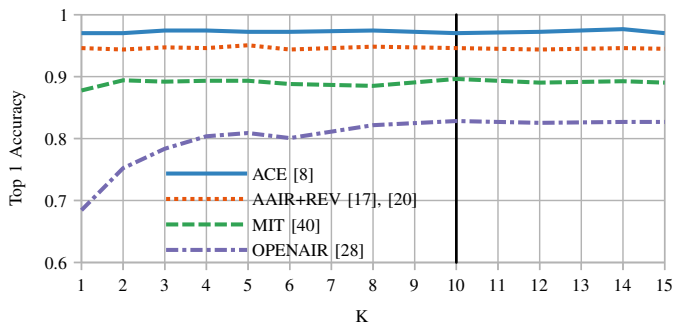


Fig. 4: Top-1 environment matching accuracy in dependence of the number of reference samples for prototype computation  $K$ . The out-of-distribution OPENAIR environments require a larger number of reference samples.

small to large environments. The test data is obtained from our data generator, configured to use multiple compressions with randomly selected codec and bitrate as specified in Sec. IV-B1.

Figure 5a shows the Top- $\{1,2,3\}$  accuracy results for single, double and triple compression. As expected, the accuracy degrades with increasing number of compressions. However, the total performance remains high even for Top-1 predictions. The accuracy is 0.9351 for double compression and 0.9052 for triple compression, which is only moderately lower than 0.9657 for single compression. For Top- $\{2,3\}$  predictions, the performance never falls below 0.9590. The experiment thus shows a good generalization to longer compression chains.

3) *Unseen Compression Codecs*: Fast progress in audio compression research might lead to the case that EnvId must perform inference on compression codecs that it has not been trained for.

The experiments are performed on the identically trained Gamper\* backbone as in the previous experiment. The evaluation is again performed on the MIT-based test set from Tab. II, but this time compressed with two codecs that were

not seen during training, namely Vorbis as an established analytic compressor and EnCodec [5] from Meta Research<sup>®</sup> as a relevant neural network-based compressor. Both codecs are evaluated with low, middle and high quality settings.

Figure 5b shows the result for Vorbis, and Fig. 5c shows the results for EnCodec. The accuracy on Vorbis compression is very close to 1, which is understandable, as it targets mid to high quality output where the lowest available bitrate is still as high as 16 kbps. In contrast, EnCodec [5] has a higher impact on the performance. While the Top-1 accuracies on the high (24 kbps) and mid (6 kbps) quality settings are 0.9216 and 0.8299, it drops to 0.5701 for the low (1.5 kbps) quality setting. The low accuracy on such an extremely low bitrate is not surprising: the lowest available bitrate in the training set are 4.75 kbps with AMR-NB, hence EnvId has to simultaneously deal with unseen compression artifacts at an unseen low bitrate.

Overall, EnvId is quite robust to unseen compression codecs, even at low bitrates of 24 kbps or even 6 kbps. Only EnCodec’s strongest compression of 1.5 kbps considerably degrades the identification accuracy.

4) *Unseen Noise Impact*: The background noise may considerably vary in the test data. To evaluate EnvId’s generalization ability towards real environmental background noise, a selection of 4 publicly available noise sources is used that cover a passing train<sup>2</sup>, falling rain<sup>3</sup>, and sounds of a crowded airport<sup>4</sup> and exhibition hall<sup>5</sup>.

The test data set is identically composed to the previous experiments, with the only difference that instead of compression traces these background noise sources are added. Per test sample, one of the noise patterns is randomly selected, and added with a SNR of 50, 25, or 0.

<sup>2</sup><https://freesound.org/people/theplax/sounds/615849/>

<sup>3</sup><https://freesound.org/people/straget/sounds/531947/>

<sup>4</sup><https://freesound.org/people/arnaud%20coutancier/sounds/424362/>

<sup>5</sup><https://freesound.org/people/BockelSound/sounds/487600/>



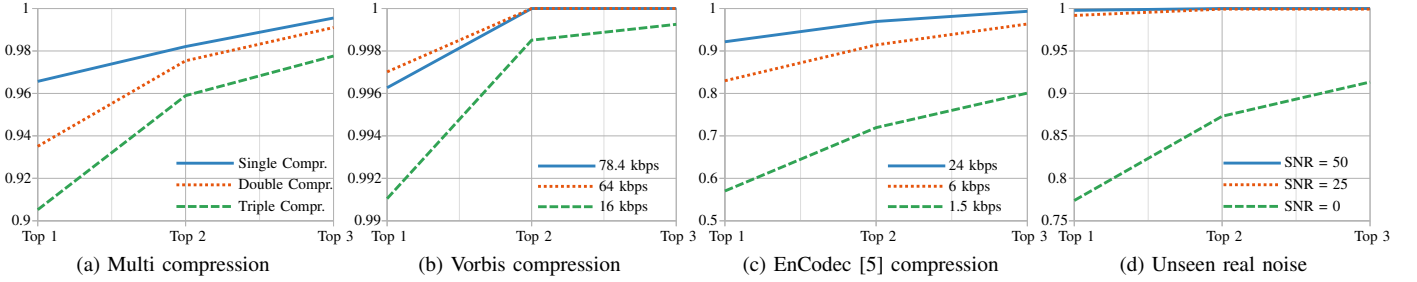


Fig. 5: Top- $\{1,2,3\}$  accuracy for few-shot environment identification under different degradation factors unseen during training. We provide benchmarks for multi compression runs (Fig. 5a), high, mid and low quality settings of the unseen Vorbis (Fig. 5b) and neural EnCodec [5] compression codecs (Fig. 5c), and unseen real environmental background noise (Fig. 5d).

The evaluation result is shown in Fig. 5d. Small and medium noise levels have little influence as EnvId’s Top-1 accuracy is close to 1. However, strongly degraded signals cause the accuracy to fall to 0.7739, 0.8731 and 0.9134 for the Top-1, Top-2 and Top-3 predictions, respectively. Nevertheless, the results are remarkable when considering that the noise pattern is unseen and the distortion of the signal is extremely high.

#### D. Recording Position Mismatch

The actual position of the microphones in the room is a subtle, yet quite impactful issue that has been barely addressed in related works (cf. Sec. II).

If reference audio samples from candidate environments are collected during the investigation process, it must be assumed that the recording position of the  $K$  collected reference samples is at least somewhat different from the query signal. To our knowledge, the impact of this issue has not been quantified before. We provide a benchmark and dataset with synthetic data of enclosed spaces of varying recording positions in differently shaped rooms. The evaluation is again performed with the best EnvId setting, fine-tuned with identical hyperparameters as above.

1) *Microphone Position Data Set*: To the best of our knowledge, there is no dataset that provides a grid of real AIR measurements with known positions for a large number of recording locations. Hence, we simulate enclosed spaces with pyroomacoustics [36]. We consider rooms within a length interval of  $l_r \in [1, 50]$  m and height  $h_r \in [2, 5]$  m in steps of 10 cm. Three common room shapes are *corridor*, *rectangle*, and *square* rooms, where we define the fraction  $f$  of width over length as  $f \in [0.1, 0.3]$  for corridor,  $f \in [0.4, 0.7]$  for rectangle, and  $f \in [0.8, 1]$  for square.

Different floor and wall characteristics are simulated with an absorption coefficient  $c_a \in [0.1, 0.8]$ . AIR measurements are sampled from a equidistant  $5 \times 5$  grid per room to uniformly cover potential microphone positions. The distance between the outer edges of the grid to the corresponding nearest wall is set to 30 cm. For this first study, we focus on the practically relevant scenario of some speaker during a telephone conversation or the recording of voice messages. The relative distance between the microphone and the speaker is thus set to a fixed size of 10 cm, and the microphone is always positioned 1.7 m above the ground floor. The speaker

orientation is always set towards the room center and the microphone is set inversely. This preserves the comparability of different grid positions.

Our final training/validation set consists of distinct random samples of 45/15 rooms from each of the 3 shape categories uniformly sampled from the whole volume range, which leads to 135/45 rooms per set. For each room, absorption coefficients are randomly sampled. AIR measurements are simulated for each of the  $5 \times 5$  grid positions, yielding a total of 3375/1125 training/validation AIRs. Each AIR is convolved with each of 25/19 anechoic speech samples from a subset of the ACE training and validation pool (Tab. I). This leads to a total of about 84k/21k training/validation samples. To approximate real world scenarios, we again include additive white noise and single compression degradation of varying strength as in the previous experiments.

2) *Recording Position Evaluation*: The test set is constructed with a volume range of  $V \in [10, 3750]$  m<sup>3</sup>, as 3750 m<sup>3</sup> is the maximum possible volume for a *corridor* room in our setting. We sample one room per shape category for 10 volumes uniformly distributed over the full range to yield 30 test rooms in total. The absorption coefficient is fixed to  $c_a = 0.1$  for medium absorption [36]. The fixed absorption coefficient in the test set enables an isolated analysis of the impact of changing recording positions. Per room, AIRs measured from the  $5 \times 5$  grid positions are convolved each with a subset of 16 samples from the TSP test pool (Tab. I), yielding 12k samples in total. The evaluation tests each of the 25 positions against all other recording positions.

When averaging over all positions in all rooms per room category, then *corridor* rooms are easiest to identify with an average accuracy of 0.7715, followed by *rectangle* and *square* rooms with average accuracies of 0.7648 and 0.7608. The results for each individual position are visualized in Fig. 6 for the three room shape categories *corridor* (left), *rectangle* (middle), and *square* (right). Overall, the accuracy tends to increase at locations that are closer to the walls. For example, the average center accuracies are 0.6375, 0.6875 and 0.7063 for *corridor*, *rectangle* and *square* rooms, but average accuracies at walls are 0.7663, 0.7687 and 0.7606. For *rectangle* and *square* rooms it is particularly notable that the most difficult positions are the ones along the middle column. We hypothesize that the more distinct early reflections in the

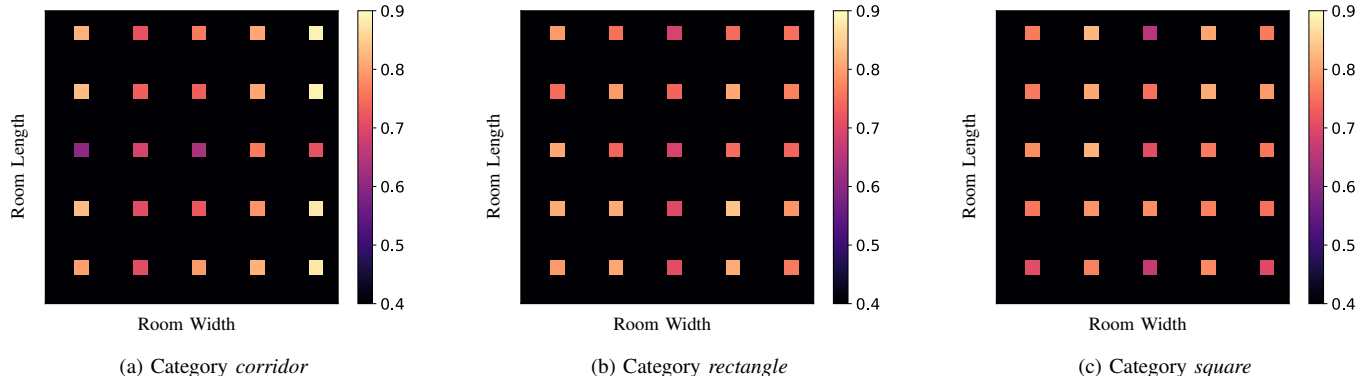


Fig. 6: Mean accuracy for specific microphone positions on a uniformly sampled  $5 \times 5$  grid for the categories *corridor*, *rectangle* and *square*. For visualization, all heatmaps are scaled to quadratic size. Environments for audio samples recorded closer to boundaries are on average easier to identify. The total accuracy thus decreases for wider room widths from left to right.

Room Category	RMSE			Mean Targets
	Clean	Compr.	Noise	
Corridor	0.2640	0.2723	0.2748	0.6497
Rectangle	0.1692	0.1921	0.2157	0.4930
Square	0.1553	0.1777	0.2117	0.4125

TABLE IV: Results for the regression of  $RT_{60}$  on our synthetic dataset. The RMSE and mean target  $RT_{60}$  are reported for medium reflecting spaces with randomly sampled absorption coefficients  $0.1 \leq c_a \leq 0.8$ . The results are grouped by the room categories *corridor*, *rectangle*, and *square*.

Signal Degradation	Accuracy			
	2-class	3-class	5-class	10-class
Clean	0.9706	0.9519	0.8566	0.7808
Compression	0.8872	0.8410	0.7045	0.6593
Noise	0.8298	0.7930	0.6605	0.5999

TABLE V: Results for classifying rooms in 2, 3, 5, or 10 size categories via thresholding on the volume estimate.

AIR for recordings close to walls lead to more characteristic features, which makes environment identification easier. This is in line with the observation that the overall accuracies are highest on *corridor* rooms, where the walls are closest relative to the volume of the room.

We also investigate the impact of compression and noise with degradation settings as described in Sec. IV-B1. For compression, the averaged accuracy over all recording positions drops to 0.6458, 0.6163 and 0.6340 for *corridor*, *rectangle* and *square* rooms. Noise has an even stronger impact and decreases the values down to 0.5298, 0.4898 and 0.5118, respectively.

Overall, these first results are promising, even though this experiment is limited in scope due to the fixed absorption coefficients. The results demonstrate that the microphone location is an important factor that should be considered in future research and in practice.

### E. Blind Environment Parameter Estimation

In forensic investigations may occur cases where there is no hypothesis about candidate recording locations. In such an unconstrained scenario, the only possible contribution is to estimate recording parameters from the input sample. EnvId can provide such an estimate as a regression result. We demonstrate this for the room volume  $V$  and the  $RT_{60}$  parameter, which are popular quantities in related work (cf. Sec. II). We use the same training setup as in the previous experiment, with the only difference that we use a regression head for the parameter prediction (cf. Sec. III-A4).

We first compare EnvId’s regression capability to the recently proposed estimator by Götz *et al.* [13] who also apply representation learning techniques.

In detail, they use contrastive learning with an upstream encoder network to obtain embeddings for room volume and  $RT_{60}$ . These embeddings are fed to a downstream network to classify the room volume as small or large, and to regress the  $RT_{60}$ . With the help of the authors, we recreate the dataset by Götz *et al.* [13] according to their protocol. The training set consists of simulated rooms of uniformly distributed volumes  $V \in [27, 500]m^3$  and randomly sampled absorption coefficients. The test set consists of 1000 AIRs, *i.e.*, 10 AIRs from 100 simulated rooms as described in their work [13].

When running this experiment, EnvId achieves a root mean squared error (RMSE) of 0.2129 for  $RT_{60}$  and a remarkable volume classification accuracy of 0.9998. Both values outperform the work by Götz *et al.*, who report a minimum RMSE of 0.2146 for  $RT_{60}$  and a maximum volume classification accuracy of 0.7422.

To provide further results for EnvId, we also report results for the synthetic room set from Sec. IV-D1 and Sec. IV-D2 which covers a larger volume range of  $V \in [10, 3750]m^3$  and includes additive noise and compression. For this experiment, we further randomly sample absorption coefficients  $c_a$  between 0.1 and 0.8 for all rooms.

We first evaluate the influence of room shape on the estimation of the  $RT_{60}$  parameter. The results are shown in

Tab. IV. Both the RMSE and  $RT_{60}$  mean values of the targets are reported grouped by shape category. As is reflected by the mean target  $RT_{60}$ , the  $RT_{60}$  naturally increases for more elongated rooms in our set. Equally, the RMSE increases, such that *corridor* rooms exhibit higher RMSE scores than *rectangle* and especially *square* rooms. Compression and added noise slightly reduce the performance. The average RMSE increases by 1.79 percentage points (pp) for compression and by 3.79 pp for noise. These findings are in line with the results in the previous Section.

To provide an intuition about the quality of the volume predictions, we extend the evaluation approach by Götz *et al.* [13]. As previously discussed, they use the volume estimate to classify room sizes as small or large with a maximum accuracy of 0.7422, while EnvId exhibits a notable strong performance with a classification accuracy of 0.9998 on the same data and task. In this experiment, we generalize this approach and evenly divide the volume range of our data in  $n \in \{2, 3, 5, 10\}$  classes. The classification itself is done via thresholding. Table V shows the results. The two class task is solved with a high accuracy of 0.9706. Added compression decreases the accuracy to 0.8872, added noise to 0.8298. Naturally, accuracies decrease for increasing numbers of size categories. However, for the finest problem granularity of 10 classes, EnvId still achieves accuracies of 0.7808, 0.6593 and 0.5999 for clean, compressed and noisy inputs.

We take this as evidence that EnvId with added regression head is able to outperform the dedicated state-of-the-art regression network by Götz *et al.* [13]. EnvId is able to blindly extract relevant cues about recording location characteristics from the internal representations used for few-shot classification, also under signal impacting factors like noise or compression.

## V. CONCLUSION

DL tools are increasingly moving into the focus of police authorities to support criminal investigations. However, it remains an open challenge to develop tools that are flexible and robust enough to meet practical requirements. In particular, the identification of recording environments from single audio samples is challenging due to the many practical challenges in this seemingly straightforward task.

In this work, we propose EnvId as a step towards practically applicable recording environment identification. EnvId is an end-to-end trainable framework for few-shot recording location identification which supports recording parameter estimation. EnvId addresses a number of practically relevant requirements, including open-set identification and identification of data with unknown degradations. With the help of EnvId, we also explore the so-far neglected, but practically very important issue of a mismatch in recording locations. Here, our experiments quantitatively show that it is notably easier to identify a room from mismatched recording locations when they were done closer to the walls.

## REFERENCES

- [1] Mohammadreza Azimi and Utz Roedig. Room Identification with Personal Voice Assistants. In *European Symposium on Research in Computer Security*, pages 317–327. Springer, 2021.
- [2] Gianmarco Baldini and Irene Amerini. Microphone Identification based on Spectral Entropy with Convolutional Neural Network. In *International Workshop on Information Forensics and Security*, pages 1–6. IEEE, 2022.
- [3] Malte Baum, Luca Cuccovillo, Artem Yaroshchuk, and Patrick Aichroth. Environment Classification via Blind Roomprints Estimation. In *International Workshop on Information Forensics and Security*, pages 1–6. IEEE, 2022.
- [4] Joon Son Chung, Jaesung Huh, Seongkyu Mun, Minjae Lee, Hee Soo Heo, Soyeon Choe, Chiheon Ham, Sunghwan Jung, Bong-Jin Lee, and Icksang Han. In Defence of Metric Learning for Speaker Recognition. In *INTERSPEECH*, pages 2977–2981, 2020.
- [5] Alexandre Défossez, Jade Copet, Gabriel Synnaeve, and Yossi Adi. High Fidelity Neural Audio Compression. *Transactions on Machine Learning Research*, 2023.
- [6] Shuwen Deng, Wolfgang Mack, and Emanuël AP Habets. Online Blind Reverberation Time Estimation Using CRNNs. In *INTERSPEECH*, pages 5061–5065, 2020.
- [7] Alexey Dosovitskiy, Lucas Beyer, Alexander Kolesnikov, Dirk Weissenborn, Xiaohua Zhai, Thomas Unterthiner, Mostafa Dehghani, Matthias Minderer, Georg Heigold, Sylvain Gelly, et al. An Image is Worth 16x16 Words: Transformers for Image Recognition at Scale. In *International Conference on Learning Representations*, 2021.
- [8] James Eaton, Nikolay D Gaubitch, Alastair H Moore, and Patrick A Naylor. Estimation of Room Acoustic Parameters: The ACE Challenge. *IEEE/ACM Transactions on Audio, Speech, and Language Processing*, 24(10):1681–1693, 2016.
- [9] Hannes Gamper. Blind C50 Estimation from Single-Channel Speech Using a Convolutional Neural Network. In *International Workshop on Multimedia Signal Processing*, pages 1–6. IEEE, 2020.
- [10] Hannes Gamper and Ivan J Tashev. Blind Reverberation Time Estimation Using a Convolutional Neural Network. In *16th International Workshop on Acoustic Signal Enhancement*, pages 136–140. IEEE, 2018.
- [11] Andrea F Genovese, Hannes Gamper, Ville Pulkki, Nikunj Raghuvanshi, and Ivan J Tashev. Blind Room Volume Estimation from Single-Channel Noisy Speech. In *International Conference on Acoustics, Speech and Signal Processing*, pages 231–235. IEEE, 2019.
- [12] Philipp Götz, Cagdas Tuna, Andreas Walther, and Emanuël AP Habets. Blind Reverberation Time Estimation in Dynamic Acoustic Conditions. In *International Conference on Acoustics, Speech and Signal Processing*, pages 581–585. IEEE, 2022.
- [13] Philipp Götz, Cagdas Tuna, Andreas Walther, and Emanuël AP Habets. Contrastive Representation Learning for Acoustic Parameter Estimation. In *International Conference on Acoustics, Speech and Signal Processing*, pages 1–5. IEEE, 2023.
- [14] Kaiping He, Xiangyu Zhang, Shaoqing Ren, and Jian Sun. Deep Residual Learning for Image Recognition. In *Conference on Computer Vision and Pattern Recognition*, pages 770–778. IEEE, 2016.
- [15] Calum Heggan, Sam Budgett, Timothy Hospedales, and Mehrdad Yaghoubi. Metaaudio: A Few-Shot Audio Classification Benchmark. In *International Conference on Artificial Neural Networks*, pages 219–230. Springer, 2022.
- [16] Christopher Ick, Adib Mehrabi, and Wenyu Jin. Blind Acoustic Room Parameter Estimation Using Phase Features. In *International Conference on Acoustics, Speech and Signal Processing*, pages 1–5. IEEE, 2023.
- [17] Marco Jeub, Magnus Schafer, and Peter Vary. A Binaural Room Impulse Response Database for the Evaluation of Dereverberation Algorithms. In *International Conference on Digital Signal Processing*, pages 1–5. IEEE, 2009.
- [18] Peter Kabal. TSP Speech Database. *McGill University, Database Version*, 1(0):09–02, 2002.
- [19] Diederik P Kingma and Jimmy Ba. Adam: A Method for Stochastic Optimization. In *3rd International Conference for Learning Representations*, 2015.
- [20] Keisuke Kinoshita, Marc Delcroix, Takuya Yoshioka, Tomohiro Nakatani, Emanuel Habets, Reinhold Haeb-Umbach, Volker Leutnant, Armin Sehr, Walter Kellermann, Roland Maas, et al. The REVERB Challenge: A Common Evaluation Framework for Dereverberation and Recognition of Reverberant Speech. In *Workshop on Applications of Signal Processing to Audio and Acoustics*, pages 1–4. IEEE, 2013.
- [21] Zhuang Liu, Hanzi Mao, Chao-Yuan Wu, Christoph Feichtenhofer, Trevor Darrell, and Saining Xie. A ConvNet for the 2020s. In *Conference on Computer Vision and Pattern Recognition*, pages 11976–11986. IEEE/CVF, 2022.
- [22] B LOGAN. Mel Frequency Cepstral Coefficients for Music Modelling. In *Proc. International Symposium on Music Information Retrieval*, 2000.

- [23] Alastair H Moore, Mike Brookes, and Patrick A Naylor. Room Geometry Estimation From a Single Channel Acoustic Impulse Response. In *21st European Signal Processing Conference*, pages 1–5. IEEE, 2013.
- [24] Alastair H Moore, Mike Brookes, and Patrick A Naylor. Roomprints for Forensic Audio Applications. In *Workshop on Applications of Signal Processing to Audio and Acoustics*, pages 1–4. IEEE, 2013.
- [25] Alastair H Moore, Mike Brookes, and Patrick A Naylor. Room Identification Using Roomprints. In *54th International Conference: Audio Forensics*. Audio Engineering Society, 2014.
- [26] Alastair H Moore, Patrick A Naylor, and Mike Brookes. Room Identification Using Frequency Dependence of Spectral Decay Statistics. In *International Conference on Acoustics, Speech and Signal Processing*, pages 6902–6906. IEEE, 2018.
- [27] Denise Moussa, Germans Hirsch, Sebastian Wankerl, and Christian Riess. Point to the Hidden: Exposing Speech Audio Splicing via Signal Pointer Nets. In *Proc. INTERSPEECH 2023*, pages 5057–5061, 2023.
- [28] Damian T Murphy and Simon Shelley. OpenAIR: An Interactive Auralization Web Resource and Database. In *129th Audio Engineering Society Convention*. Audio Engineering Society, 2010.
- [29] Arsha Nagrani, Joon Son Chung, and Andrew Zisserman. VoxCeleb: A Large-Scale Speaker Identification Dataset. *INTER\_SPEECH*, pages 2616–2620, 2017.
- [30] Constantinos Papayiannis, Christine Evers, and Patrick A Naylor. Discriminative Feature Domains for Reverberant Acoustic Environments. In *International Conference on Acoustics, Speech and Signal Processing*, pages 756–760. IEEE, 2017.
- [31] Constantinos Papayiannis, Christine Evers, and Patrick A Naylor. End-to-end Classification of Reverberant Rooms Using DNNs. *IEEE/ACM Transactions on Audio, Speech, and Language Processing*, 28:3010–3017, 2020.
- [32] Adam Paszke, Sam Gross, Francisco Massa, Adam Lerer, James Bradbury, Gregory Chanan, Trevor Killeen, Zeming Lin, Natalia Gimelshein, Luca Antiga, Alban Desmaison, Andreas Kopf, Edward Yang, Zachary DeVito, Martin Raison, Alykhan Tejani, Sasank Chilamkurthy, Benoit Steiner, Lu Fang, Junjie Bai, and Soumith Chintala. PyTorch: An Imperative Style, High-Performance Deep Learning Library. In *Advances in Neural Information Processing Systems*, pages 8024–8035, 2019.
- [33] Nils Peters, Howard Lei, and Gerald Friedland. Name That Room: Room Identification Using Acoustic Features in a Recording. In *20th ACM International Conference on Multimedia*, pages 841–844, 2012.
- [34] Ilija Radosavovic, Raj Prateek Kosaraju, Ross Girshick, Kaiming He, and Piotr Dollár. Designing Network Design Spaces. In *Conference on Computer Vision and Pattern Recognition*, pages 10428–10436. IEEE/CVF, 2020.
- [35] Davide Salvi, Mirco Pezzoli, Sara Mandelli, Paolo Bestagini, and Stefano Tubaro. Are you Really Alone? Detecting the use of Speech Separation Techniques on Audio Recordings. In *International Workshop on Information Forensics and Security*, pages 1–6. IEEE, 2023.
- [36] Robin Scheibler, Eric Bezzam, and Ivan Dokmanić. Pyroomacoustics: A Python Package for Audio Room Simulation and Array Processing Algorithms. In *International Conference on Acoustics, Speech and Signal Processing*, pages 351–355. IEEE, 2018.
- [37] Jake Snell, Kevin Swersky, and Richard Zemel. Prototypical Networks for Few-Shot Learning. *Advances in Neural Information Processing Systems*, 30, 2017.
- [38] Mingxing Tan and Quoc Le. EfficientNet: Rethinking Model Scaling for Convolutional Neural Networks. In *International Conference on Machine Learning*, pages 6105–6114. PMLR, 2019.
- [39] TorchAudio. torchaudio.transforms — TorchAudio 0.10.0 Documentation, accessed: 2023-05-25. <https://pytorch.org/audio/0.10.0/>.
- [40] James Traer and Josh H McDermott. Statistics of Natural Reverberation Enable Perceptual Separation of Sound and Space. *Proceedings of the National Academy of Sciences*, 113(48):E7856–E7865, 2016.
- [41] Ashish Vaswani, Noam Shazeer, Niki Parmar, Jakob Uszkoreit, Llion Jones, Aidan N Gomez, Łukasz Kaiser, and Illia Polosukhin. Attention is All You Need. *Advances in Neural Information Processing Systems*, 30, 2017.
- [42] Yu Wang, Nicholas J Bryan, Mark Cartwright, Juan Pablo Bello, and Justin Salamon. Few-Shot Continual Learning for Audio Classification. In *International Conference on Acoustics, Speech and Signal Processing*, pages 321–325. IEEE, 2021.
- [43] Piper Wolters, Chris Careaga, Brian Hutchinson, and Lauren Phillips. A Study of Few-Shot Audio Classification. *GHC*, 2020.
- [44] Ziyue Xiang, Paolo Bestagini, Stefano Tubaro, and Edward J Delp. Forensic Analysis and Localization of Multiply Compressed MP3 Audio Using Transformers. In *IEEE International Conference on Acoustics, Speech and Signal Processing*, pages 2929–2933. IEEE, 2022.
- [45] Weidi Xie, Arsha Nagrani, Joon Son Chung, and Andrew Zisserman. Utterance-Level Aggregation for Speaker Recognition in the Wild. In *International Conference on Acoustics, Speech and Signal Processing*, pages 5791–5795. IEEE, 2019.
- [46] Shilei Zhang, Yong Qin, Kewei Sun, and Yonghua Lin. Few-Shot Audio Classification with Attentional Graph Neural Networks. In *Interspeech*, pages 3649–3653, 2019.
- [47] James Zjalic. *Digital Audio Forensics Fundamentals: From Capture to Courtroom*. CRC Press, 2020.